Reac Kinet Mech Cat (2015) 115:389–400
DOI 10.1007/s11144-015-0845-0

Photocatalytic degradation of orange II on the novel hetero-system WS_2/TiO_2 under UV light

S. Bassaid · B. Bellal · M. Trari

Received: 12 November 2014 / Accepted: 10 February 2015 / Published online: 19 February 2015

Abstract The photodegradation of orange II (OII) is successfully achieved on the new hetero-system WS_2/TiO_2 under UV illumination. The nano sized bi-functional catalyst is prepared by sol gel and calcined at $\sim$450 °C. The X-ray diffraction shows noticeably broad peaks and TiO_2 is therefore less crystallized with the anatase phase. The sensitizer WS_2 presents a direct optical transition at 1.72 eV. The Mott–Schottky plot (C^{-2}–V) is characteristic of *n* type conduction from which a flat band potential of 0.17 V_{SCE} and a donor density of 5.30×10^{17} cm^{-3} are determined. An energy band diagram is established, predicting an electron transfer from WS_2 to TiO_2; the injection process is confirmed by the photocurrent measurements at different concentrations. Upon increasing the mass of WS_2, the activity increases and the best performance occurs on 30 % WS_2/TiO_2. A conversion of 98 % is reported in aerated solution for OII concentration of 10 ppm in less than 90 min. The oxidation follows a first order kinetic with a rate constant of 4.8×10^{-2} min^{-1}.

Keywords Hetero-system WS_2/TiO_2 · Orange II · Photocatalytic degradation · Kinetic

Introduction

Conventionally, wastewaters are treated by physical and/or biological methods that reduce the pollution level, but not enough to comply with the directives of the

S. Bassaid · B. Bellal · M. Trari (✉)
Laboratory of Storage and Valorization of Renewable Energy, Faculty of Chemistry (USTHB), BP 32, 16111 Algiers, Algeria
e-mail: solarchemistry@gmail.com

World Health Organization [1, 2]. In this respect, the advanced oxidation process (AOP) has emerged as a promising technique for the remediation of the aquatic environment, particularly for the effluents produced by the textile industry [3–6]. The SC-liquid junction may be viewed as infinity of micro-photo-electrochemical (PEC) cells. TiO_2 is a catalyst of choice for many applications and remains very popular owing of its superior activity, chemical stability and non-toxicity. It can practically degrade many hazardous by-products including dyes, drugs and pesticides [7, 8] or produce hydrogen from water [9]. However, TiO_2 based solar devices are efficient at short wavelengths (<400 nm) where only 5 % of the solar spectrum accounts for the UV radiation. Many efforts have been focused on hetero-systems which could not only extend the spectral response of wide band gap semiconductors (SCs) toward lower energies but also inhibit the charge recombination and in this way increase the photocatalytic performance [10]. TiO_2 can mediate the electron transfer and plays a crucial role when the potential of its conduction band (CB) is less cathodic than that of the photosensitizer [11].

On the other hand, the layered chalcogenides MX_2, where M is commonly a transition metal and X an element of group VI_A (X = S, Se and Te), have been actively used in PEC applications [12]. In this category, WS_2 is an attractive material for the solar energy conversion because it combines a narrow band gap, a chemical inertness over a fair pH range and occurs in *n*- as well in *p*-types [13]. In contrast to oxides that have a valence band (VB) deriving from O^{2-}: *2p* parentage, WS_2-VB is made up of less electronegative S: *3p* orbital. This leads to a lower gap and a CB of cationic character with a high reducing ability. The optical transition is of *d–d* characteristic and involves lower and upper bands of W^{4+}: *5d*: orbital. Consequently, the bond W–S is unaffected and the photocorrosion is less pronounced. In addition, the position of the bands does not change with pH and can be positioned adequately with respect to those of TiO_2. The PEC properties of WS_2 and the position of the band edges, imposed by the crystal structure itself, are essential to predict the mechanistic and transport of the charges carriers. With a gap of $\sim$1.8 eV, WS_2 can absorb $\sim$50 % of the sunlight and possesses high absorption coefficients ($\sim 10^5$ cm^{-1}) [14].

The main goal of this work is to report the preparation of the hetero-system TiO_2/WS_2 by sol gel and its PEC characterization. As an application, the photocatalytic performance is successfully tested toward the oxidation of orange II (OII) upon UV light on the bi-functional hetero-system under short circuited conditions. OII is a model molecule with weak biodegradability, it is widely used in the textile industry because of its coloring properties and its degradation is of potential significance. The photocatalytic activity is dependent on many parameters among which the OII concentration and WS_2 loading.

Experimental

The hetero-system TiO_2/WS_2 is synthesized by sol gel; titanium iso-propoxyde {$Ti(OC_3H_7)_4$, Aldrich, 97 %}, ethanol (Fluka, 98 %) and methanol (Fluka, >99.5 %) are used as starting reagents. An equimolar mixture of ethanol/methanol

is introduced in a Pyrex beaker (250 mL capacity) and $Ti(OC_3H_7)_4$ is added dropwise. Then, the desired amount of WS_2 is added. The proportions of the sensitizer (WS_2) with respect to the mass of TiO_2 (prepared alone in a first part) were 10 % (0.167 g), 20 % (0.334 g) and 30 % (0.501 g). The resulting mixture is heated during 3 h at 75 °C, after which hot water is added dropwise. After gelling, the samples were dried overnight at 110 °C and then heat-treated in air for 2 h at 450 °C with a heating rate of 3 °C/min. To confirm the formation of the phases, X-ray diffraction (XRD) is performed with a Siemens diffractometer (Model D-5000) using Cu K_α radiation. BET surface areas are determined from nitrogen adsorption at 77 K using a Micromeritics apparatus (Coulter SA 3100 and Belsorp-mini porosimeter); the samples are outgassed at 140 °C (4 h) to vacuum (10^{-4} Pa) in order to have a clean surface.

The optical absorption spectra are recorded with a double beam spectrophotometer (Specord 200 Plus) equipped with an integrating sphere, PTFE is used as reference. The point of zero zeta potential (pzzp) of WS_2 is determined from the equilibrium pH of an aqueous solution containing a powder suspension; a value of ~ 1 is obtained.

WS_2 is mechanically soft with poor sintering. It is cold pressed into circular pellets ($\varnothing = 13$ mm, thickness ~ 1 mm) under a pressure of 4 tons cm^{-2} and heated at 300 °C in evacuated Pyrex ampoule, the compactness approximates 70 %. Ohmic contact onto the back pellets is made by soldering copper wires with silver paint. The working electrodes (WE) are prepared by encapsulating the pellets in glass holders. Electrochemical (EC) and PEC characterizations are carried out in a closed cell with a three electrode arrangement using Pt sheet (1 cm^2) as auxiliary electrode. All potentials are given with respect to a saturated calomel electrode (SCE) and controlled with a PGZ301 potentiostat (Radiometer analytical). WS_2 is illuminated with a tungsten lamp (200 W) through an optical window. The differential capacitance is measured at a frequency of 10 kHz.

The photocatalytic tests are done in batch mode. 50 mg of TiO_2/WS_2 are dispersed by magnetic stirring in 100 mL of OII solution (10 mg/L). The temperature is regulated at 25 °C with a thermostated bath. The powder suspension is achieved by magnetic stirring; ~ 2 h is required to reach the dark adsorption equilibrium. The light source consists of a high pressure mercury lamp (HPK 125 W Phillips), mounted on the central axis of a quartz reactor. The aliquots are withdrawn at regular times, subjected to a vigorous centrifugation (3000 rpm, 15 mn) to remove the solid particles and filtered through a 0.45-mm Millipore filter. The disappearance of OII is followed by UV–Visible spectrophotometry (Shimadzu 1800, $\lambda_{max} = 484$ nm) using 1 cm quartz cell. The photocatalytic yield is calculated from the relation:

$$\eta = 100 \times (C_0 - C_t)/C_0 \quad (1)$$

Here, C_0 is the initial concentration and C_t the concentration after irradiation for time (t). No OII is degraded in the dark and all solutions are made up with CO_2 free distilled water.

Results and discussion

Structure and optical properties of WS_2

TiO_2 presents three crystallographic varieties, the anatase is the most photoactive and is thermally stable up to ~500 °C, above which it converts irreversibly to the rutile variety. After calcination at 450 °C, the system is mixed phases and the XRD patterns show the peaks of WS_2 and TiO_2 anatase (Fig. 1). WS_2 is an excellent solid lubricant, which adopts the MoS_2 molybdenite structure, intermediate between the ionic rutile SnO_2 and covalent CdI_2 [15]. It has two-dimensional structure with S–W–S sandwich sheets connected to each other by Van der Waals type interactions. It crystallizes in platelet morphology, which forms layered crystal with a grey color, the structural refinement is performed with the space group $P6_3/mmc$ (No 194) in agreement with the JCPDS card No 21-1272. The structure is highly anisotropic; it is described as a cubic unit cell containing sulfur atoms at the corners and W_4S tetrahedron unit in the center.

The optical properties of WS_2 are typical of insulators and therefore not different from those of other sulfides. The fundamental absorption, which corresponds to electron excitation, is used to determine both the nature of the optical transition and its value. The relation between the gap (E_g), the absorption coefficients (α) and the incident energy ($h\nu$) is given by:

$$(\alpha h\nu)^{n} = C\left(h\nu - E_g\right) \tag{2}$$

In Eq. 2, C is a constant. For crystalline SCs, the exponent n depends on the type of transition, for direct allowed, $n = 1/2$ and for indirect allowed transition, $n = 2$. The extrapolation of the linear part $(\alpha h\nu)^n$ to the energy axis shows that the inter band transitions are directly and indirectly allowed (Fig. 2). Due to the grey color,

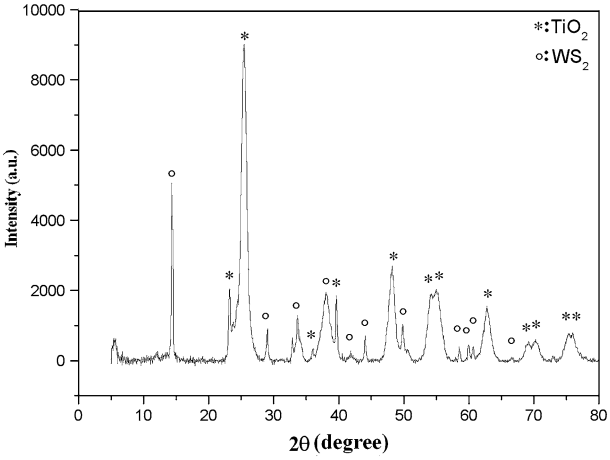

Fig. 1 X-ray diffraction pattern of the hetero-system TiO_2/WS_2 (10 %)

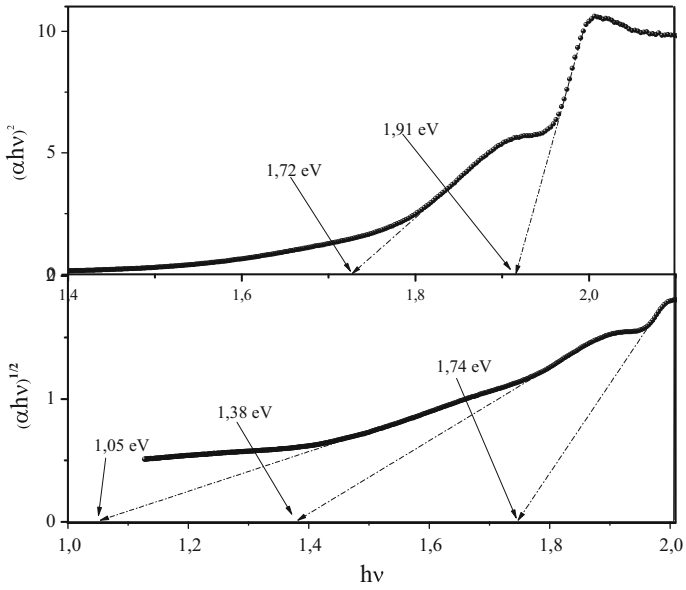

Fig. 2 Direct and indirect optical transitions of WS_2 obtained from the diffuse reflectance spectrum

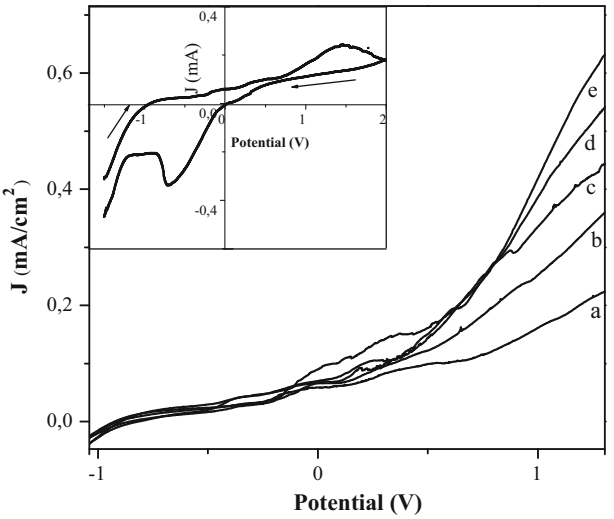

Fig. 3 The photocurrent-potential characteristics of WS_2 in aerated OII solution at different concentrations using Na_2SO_4 as support electrolyte at 25 °C, scanning rate 10 mV/s, *a* 0 ppm; *b* 5 ppm; *c* 10 ppm; *d* 15 ppm; *e* 20 ppm. *Inset* the J(V) plot of WS_2 in the dark in Na_2SO_4 electrolyte

E_g can be reasonably taken at 1.72 eV, which is attributed to the transition *5d*: W^{4+}: $e_g \rightarrow t_{2g}$. A further transition at 1.91 eV, directly allowed is presumably due to the charge transfer S^{2-}: *3p* → W^{4+}: e_g. Such energy is smaller than that observed in

oxides because of the higher energetic position of S^{2-}: *3p* orbital by ~1 eV above O^{2-}: *2p* orbital and the weak ionicity of the W–S chemical bond.

EC and PEC characterizations

The current density-potential J(V) characteristics of WS_2 are done in OII solution (10 ppm, pH ~7) using Na_2SO_4 (10^{-3} M) as support electrolyte (Fig. 3, Inset). The plot exhibits a plateau region with a dark current less than 5 μA cm^{-2} that becomes cathodically large at potentials negative of ~−0.9 V owing to hydrogen evolution. The reduction of S^{2-} to elemental sulfur appears at ~−0.5 V in close agreement with the redox potential of S/S^{2-} couple (−0.75 V). The photocurrent (J_{ph}) starts to flow at ~0 V (photocurrent onset potential: V_{on}, figure not shown) and increases toward anodic potentials, indicating *n*-type conductivity. One of the most important parameters to determine in the PEC conversion is the flat band potential (V_{fb}) under the operating conditions, it is given by the relation:

$$\frac{1}{C^2} = \left(\frac{2}{\varepsilon\varepsilon_0 e N_A}\right)\left(V - V_{fb} - kT/e\right) \tag{3}$$

Here *e* is the electronic charge, ε the dielectric constant of WS_2 (= 8) [16], ε_o the dielectric constant of vacuum (8.85×10^{-12} F m^{-1}) and *kT* the thermal energy (~26 meV at 25 °C). The intercept of the fitted line at $C^{-2} = 0$ (Fig. 4) and the slope give the potential V_{fb} (−0.77 V) and the electron density ($N_D = 5.30 \times 10^{17}$ cm^{-3}). The difference between the potentials V_{on} and V_{fb} indicates the presence of surface states within the gap region, while the positive slope confirms the *n* type behavior. WS_2 is lightly doped and the depletion width δ (~20 nm), extends over many crystallographic unit cells:

$$W = \left(\frac{2\varepsilon\varepsilon_0 \Delta V}{eN_D}\right)^{0.5} \tag{4}$$

This is advantageous in photocatalysis, where most electron/hole (e^-/h^+) pairs generated within the depletion length contribute to the photoactivity. The potential

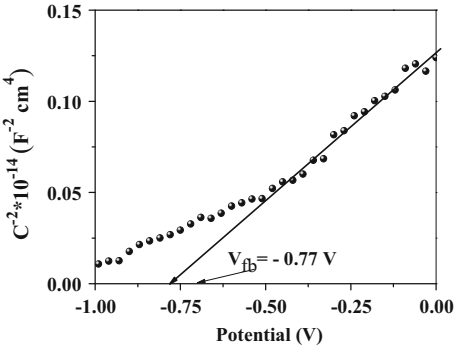

Fig. 4 The Mott-Schottky characteristic of WS_2 in Na_2SO_4 (10^{-3} M) solution plotted at 10 kHz, scanning rate 10 mV/s

V_{fb} is found to be pH-independent, and this indicates the metallic character of the electronic bands of WS_2 (see below). The energetic position of WS_2-CB with respect to vacuum is given:[1]

$$E_{CB} = 4.75 + |e|V_{fb} - E_a \quad (5)$$

The E_{CB} value is −0.87 V (3.88 eV); hence the VB is located at (0.85 V/5.6 eV = $E_{CB} + E_g$). Such a result confirms the cationic character of the electronic bands of WS_2, made up of W^{4+} *5d* orbital. This study underlines once more the role played by the crystal structure, which determines not only the position of the electronic bands, but also the width of the gap through the ionicity of the chemical bond. The electronic band are determined by *d* levels, the lower filled e_g levels providing VB though being non-bonding, whereas CB consists mainly of empty t_{2g} levels. Such electronic structure is compatible with the chemical inertness and gives WS_2 its semi-conductivity. The *d*–*d* transitions are not allowed by the Laporte rules. However, they are observed because the CB has not pure *d* character but is rather a hybridization of W^{4+}: *5d* and S^{2-}: *3p* orbitals. The CB of the anatase has not been measured because of its poorly sintered character, its value (−0.75 V) is taken from Ref. [17].

Photocatalysis

Dyes affect dramatically the aquatic life by reducing the light flux, thus inhibiting the photosynthesis; they are discharged in water and recovered by conventional methods. The adsorption is a displacement of the pollution otherwise the catalyst should be regenerated or replaced by a new one and this requires a further investment. By contrast, environmental photoelectrochemistry is an emerging technique for the water treatment [18], where the dye is converted to less harmful forms (ideally into CO_2 and H_2O). A literature survey has led to the conclusion that AOP occurs via radicals $O_2^{\bullet -}$ and/or $OH^{\bullet}$ generated respectively from photoelectrons in WS_2-CB and/or photoholes in WS_2-VB and the presence of molecular oxygen is crucial for the photodegradation. It has been observed that OII is not converted by photolysis; therefore any change in the OII concentration is due to the photocatalytic process (see below). According to the PEC characterization, the energetic diagram of the hetero-system WS_2/TiO_2 (Fig. 5) provides insights on the feasible reactions; the higher occupied molecular orbital (*HOMO*, 0.17 V) and the lower unoccupied molecular orbital (*LUMO*, −1.86 V) of OII are taken from Ref. [19]. The absorption spectrum of OII shows two main bands at 430 and 485 nm, which corresponds to the $n \rightarrow \pi*$ transition of the azo and hydrazone forms, respectively [20].

The thermodynamic requirement is such that the potential of $O_2/O_2^{\bullet -}$ couple (−0.52 V) [21] is less negative than WS_2-CB. However, the difference between the $O_2/O_2^{\bullet -}$ couple and WS_2-CB is large for a direct electron exchange and a low activity is expected since the electron transfer should occur iso-energetically. Some strategies have been attempted to overcome such drawback and a growing interest

[1] The activation E_a ($\sim$0.1 V) is determined from the conductivity measurements on sintered pellets.

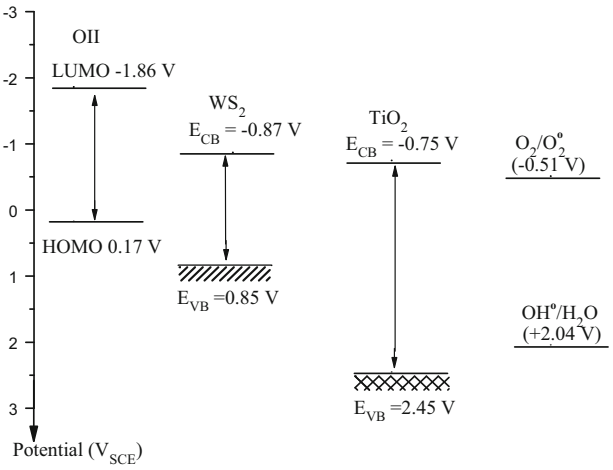

Fig. 5 The energy band diagram of the hetero-system n-WS_2/n-TiO_2 in the orange II solution at pH $\sim$ 6

has been paid to hetero-systems [22, 23]. As mentioned above, coupled SCs enhance the photocatalytic efficiency by extending the spectral photoresponse toward longer wavelengths and hinder the loss of (e^-/h^+) pairs [24].

WS_2-CB is pH insensitive whereas TiO_2-CB changes usually by -0.06 V pH^{-1}, we have exploited this property to have an optimal band bending at neutral pH. Owing to the adequate position of its CB, TiO_2 provides a bridge between WS_2 and the $O_2/O_2^{\bullet}$ couple since WS_2-CB (-0.87 V) is more cathodic than TiO_2-CB (-0.75 V) [17]. Moreover, the synthesis of TiO_2 in the presence of WS_2 in suspension byn the sol-gel method leads to intimate contact, which facilitates the electrons transfer. The photoactivity is dependent on the morphology of the bi-functional catalyst. Then, the question arises about the effect of decreasing the dimension of the crystallite on the OII oxidation. The strategy is that the charge carriers should have a lifetime as long as possible to reach the interface particularly for small polaron SCs with a low carrier mobility; this can be achieved by decreasing the path the carriers have to diffuse to reach the interface, and nano sized dimension is desirable for that purpose [25]. In this respect, the sol-gel has gained a growing popularity in the solid state chemistry for preparing particles with high surface-to-volume ratio [26]. In addition, the porous nature of TiO_2 reduces the over-voltages by increasing the active surfaces; the specific surface area determined by BET isotherms works out to be 110 m^2 g^{-1}.

The ability of excited OII to inject electrons into WS_2-CB with visible light is measured through the J(V) curves (Fig. 3). At high potentials ($>V_{fb}$) in the plateau region, the limiting current is diffusion controlled and depends only on the OII concentration i.e. the mass transport of the electro-active species toward the interface and the system is under kinetic control. Another possibility to explain the photocurrent increase can be due to the hole injection from WS_2-VB to HOMO, but this hypothesis has not been checked in our case. The dark adsorption favors the OII oxidation and is a first step in the photocatalytic process. The adsorption of azo dyes

occurs through the sulfonic groups; the primary amines groups are likely responsible for OII binding to favour its access to catalytic sites onto TiO_2 by electrostatic interactions. However, the OII adsorption is weak, less than 5 % as shown by measuring of the concentration before and after keeping the powder overnight in OII solution (10 ppm).

WS_2 is photoexcited and the electrons are injected to TiO_2-CB and subsequently transferred to dissolved oxygen which is reduced preferentially because of its redox potential (−0.50 V). Therefore, if the solution is purged with nitrogen, OII degradation is strongly inhibited. The mechanistic pathway generally accepted is the following [27]:

$$O_{2\,ads} + e^- \rightarrow O_2^{\bullet} + (H^+) \rightarrow HO_2^{\bullet} \rightarrow H_2O_2 + (e^-) \rightarrow O_2 + OH^{\bullet} + OH^- \qquad (6)$$

The illumination time is fixed at 4 h and the main parameters that influence the photoactivity are the loading of the sensitizer WS_2 and the OII concentration (C_0). The photoactivity is investigated by varying the mass of WS_2 keeping that of TiO_2 constant (Fig. 6). As expected, the performance increases with increasing the amount WS_2, due to its effective dispersion over TiO_2, which provides a high reception surface for the incident photons and in this way the contribution of a large number of (e^-/h^+) pairs. Similarly, there is an optimal concentration above which OII act as optical filter; the light is absorbed before reaching the catalyst and competes with WS_2 absorption, thus lowering the photoactivity. The half life ($t_{1/2}$), the time needed to degrade half of OII present initially, is found to be concentration dependent. The linear relation between $\ln(C_0/C_t)$ and irradiation time (t) of the photocatalytic degradation of OII obeys pseudo-first order kinetics (Fig. 7):

$$\ln C_t = -kt + \ln C_0 \qquad (7)$$

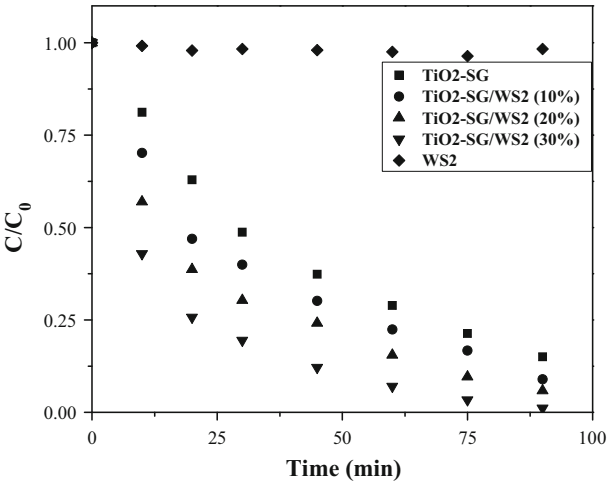

Fig. 6 Effect of WS_2 on the photocatalytic decolorization of orange II on the hetero-system TiO_2/WS_2

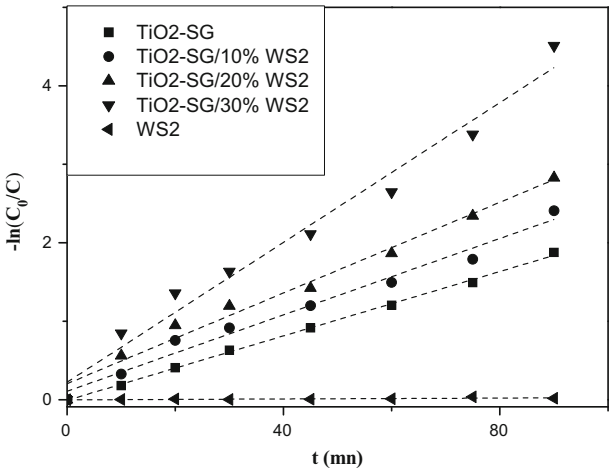

Fig. 7 Linear plots $\ln(C_0/C)$ versus illumination time of orange II on the hetero-system TiO_2/WS_2

Table 1 First order rate constant (k) and half-lives ($t_{1/2}$) for the photocatalytic degradation of orange II on TiO_2/WS_2 system

Catalysts	K_{app} (min^{-1}) × 10^2	$t_{1/2}$ (min)	R^2
TiO_2–SG	2.11	31.5	0.998
TiO_2–SG/10 %WS_2	2.61	26.7	0.990
TiO_2–SG/20 %WS_2	3.22	21.7	0.989
TiO_2–SG/30 %WS_2	4.80	14.4	0.989

The rate constants (k) and half-lives (Table 1) show that the best performance is obtained on 30 %WS_2/TiO_2 with a constant k of 4.8×10^{-2} mn^{-1}. The kinetics exhibits an initial period of relatively rapid degradation. Over time, the slopes decrease progressively and become smaller followed by the gradual cessation of the photoactivity (Fig. 6b). This tendency to saturation indicates that the layers already adsorbed are oxidized after which the process becomes governed kinetically by the diffusion of OII toward the active sites at the interface in which the radicals $OH^{\bullet}$ are generated for further adsorption/photodegradation. So, the process is self limited due to adsorbed layer and availability of photocatalytic sites. In this respect, the EC impedance would be helpful to bring insights on the interfacial process. This study is presently under way and will be consecutively reported.

Conclusion

The feasibility of WS_2 loaded TiO_2 is demonstrated for the light induced oxidation of OII in aerated aqueous solution under UV light. WS_2/TiO_2 achieves the colloidal photochemical hetero-system synthesized by sol gel with intimate contact. The choice of WS_2 is motivated by the chemical stability over a fair pH range and high

energetic position of the CB, made up of W: *5d* orbital, more cathodic than TiO_2-CB resulting in the electron transfer. The combination of the flat band potentials and optical gaps permitted to build the energetic diagram. Electron injection from OII to WS_2 upon visible illumination is confirmed by the photocurrent measurement. Oxygen improves the photoactivity considerably and the oxidation of OII obeys to first order kinetics. The photocatalytic process is governed by the diffusion of OII to active sites in which the radicals $OH^{\bullet}$ are generated.

Acknowledgments The authors would like to express their gratitude to the Faculty of Chemistry for the financial support of this research. The authors are also grateful to H. Zouaoui for his technical assistance.

References

1. Bassaid S, Chaib M, Omeiri S, Bouguelia A, Trari M (2009) Photocatlytic reduction of cadmium over $CuFeO_2$ synthesized by sol-gel. J Photochem Photobiol A 201:62–68
2. Zou L, Zhu B (2008) The synergistic effect of ozonation and photocatalysis on color removal from reused water. J Photochem Photobiol A 196:24–32
3. Petrov S, Stoichev PA (2002) Reagent ultrafiltration purification of water contaminated with reactive dyes. Filtr Sep 39(8):34–35
4. Yu H, Fugetsu B (2010) A novel adsorbent obtained by inserting carbon nanotubes into cavities of diatomite and applications for organic dye elimination from contaminated water. J Hazard Mater 177:138–145
5. Arsac F, Bianchi D, Chovelon JM, Conchon P, Ferronato C, Lair A, Sleiman M (2008) Photocatalytic degradation of organic pollutants in water and in air, an analytical approach. Mater Sci Eng C 28:722–725
6. Arslan-Alaton I (2007) Degradation of a commercial textile biocide with advanced oxidation processes and ozone. J Environ Manag 82:145–154
7. Qamar M, Gondal MA, Yamani ZH (2009) Synthesis of highly active nanocrystalline WO_3 and its application in laser-induced photocatalytic removal of a dye from water. Catal Commun 10:1980–1984
8. Yahiat S, Fourcade F, Brosillon S, Amrane A (2011) Photocatalysis as a pre-treatment prior to a biological degradation of cyproconazole. Desalination 281:61–67
9. Takimoto Y, Kitta T, Irie H (2012) Visible-light sensitive hydrogen evolution photocatalyst $ZnRh_2O_4$. Int J Hydrogen Energy 37:134–138
10. Gherbi R, Trari M, Nasrallah N (2013) Influence of light flux and hydrodynamic flow regime on the photoreduction of Cr(VI) on the $CuAl_2O_4/TiO_2$ hetero-junction. J Environ Chem Eng 1:1275–1282
11. Helaïli N, Bessekhouad Y, Bouguelia A, Trari M (2009) Visible light degradation of Orange II using xCu_yO_z/TiO_2 heterojunctions. J Hazard Mater 168:484–492
12. Bellal B, Saadi S, Koriche N, Bouguelia A, Trari M (2009) Physical properties of the delafossite $LaCuO_2$. J Phys Chem Solids 70:1132–1136
13. Benreguia N, Omeiri S, Bellal B, Trari M (2011) Visible light induced $H_2PO_4^-$ removal over $CuAlO_2$ catalyst. J Hazard Mater 192:1395–1400
14. Chen G, Li F, Fan Y, Luo Y, Li D, Meng Q (2013) A novel noble metal-free ZnS-WS_2/CdS composite photocatalyst for H_2 evolution under visible light irradiation. Catal Commun 40:51–54
15. Galasso SF (1970) Structure and properties of inorganic solids. Pergamon Press Ltd., Oxford
16. Sun S, Li Z, Chang X (2011) Synthesis and structural characterization of tungsten disulfide nanomaterials. Mater Lett 65:3164–3166
17. Bessekhouad Y, Brahimi R, Hamdini F, Trari M (2012) Cu_2S/TiO_2 hetero-junction applied to visible light Orange II degradation. J Photochem Photobiol A 248:15–23
18. Zhang YJ, Zhang L (2009) Preparation of Ru-loaded CdS/Al-HMS nanocomposites and production of hydrogen by photocatalytic degradation of formic acid. Appl Surf Sci 255:4863–4866
19. Nozik AJ, Memming R (1996) Physical chemistry of semiconductor-liquid interfaces. J Phys Chem 100(31):13061–13078

20. Park H, Choi W (2003) Visible light and Fe(III)-mediated degradation of acid Orange 7 in the absence of H_2O_2. J Photochem Photobiol A 159:241–247
21. Ortiz ME, Núñez-Vergara LJ, Squella JA (2002) Cyclic voltammetric behaviour of the O_2/O_2^- redox couple at a HMDE and its interaction with nisoldipine. J Electroanal Chem 519:46–52
22. Mazar O, Schroeder M, Tsur Y (2011) Synthesis of inside-out core-shell perovskite-type oxide nanopowder. Chem Eng J 166:1139–1143
23. Belhadi A, Boumaza S, Trari M (2011) Photoassisted hydrogen production under visible light over NiO/ZnO hetero-system. Appl Energy 88:4490–4495
24. Ge L, Liu J (2011) Efficient visible light-induced photocatalytic degradation of methyl orange by QDs sensitized CdS-Bi_2WO_6. Appl Catal B 105:289–297
25. Derbal A, Omeiri S, Bouguelia A, Trari M (2008) Characterization of new heterosystem $CuFeO_2$/SnO_2 application to visible-light induced hydrogen evolution. Int J Hydrogen Energy 33:4274–4282
26. Mozia S (2010) Application of temperature modified titanate nanotubes for removal of an azo dye from water in a hybrid photocatalysis-MD process. Catal Today 156:198–207
27. Chhor K, Bocquet JF, Colbeau-Justin C (2004) Comparative studies of phenol and salicylic acid photocatalytic degradation: influence of adsorbed oxygen. Mater Chem Phys 86:123–131